

# Warming of an elevated layer over Africa

Mark R. Jury · Kim Whitehall

Received: 7 February 2008 / Accepted: 27 May 2009 / Published online: 10 September 2009  
© Springer Science + Business Media B.V. 2009

**Abstract** This paper analyzes trends of temperatures over Africa and seeks to quantify the most significant processes. Observations of air temperature reveal significant warming trends in the 925–600 hPa layer over tropical west Africa and the east Atlantic. This is related to the influence of desert dust and biomass burning emissions on the atmospheric energy budget. We calculate a net radiative absorption of  $\sim -20 \text{ W m}^{-2}$ . The southern (northern) plume is rich in short-lived greenhouse gases (dust aerosols), and the atmospheric response, according to a simplified radiative transfer model, is a  $>3^\circ\text{C}$  heating of the 2–4 km layer. The observed pattern of warming coincides with a mixture of dust, black carbon and short-lived greenhouse gases in space, time and height. Physical forcing provides a secondary source of regional warming, with sinking motions over the Sahel. The elevated warm layer stabilizes the lower atmosphere over and west of Africa, so drying trends may be anticipated.

## 1 Introduction

Climate change has been in the forefront of studies for the past couple of decades as greenhouse gases (GHGs) warm the atmosphere. There is some debate on the scales involved in global warming, necessitating attribution studies involving historical observations, collection of field data and numerical simulations using coupled models. In order to determine the rate at which the regional climate is

---

M. R. Jury (✉)  
Physics Department, University of Puerto Rico, Mayaguez, PR 00681, USA  
e-mail: jury@uprm.edu

M. R. Jury  
University of Zululand, KwaDlangezwa, 3886, South Africa

K. Whitehall  
Caribbean Institute for Meteorology and Hydrology, Bridgetown, Barbados

changing, spatial and temporal information on atmospheric composition, structure and response are needed (Penner et al. 1998; Haywood et al. 2003; Keil and Haywood 2003). It is known that GHGs and tropospheric aerosols play a role in radiative forcing of the climate system (Tegen et al. 1996). Land use also promotes climate change (Feddema and Freire 2001; Paeth 2004) and model experiments predict a reduction in subtropical rainfall as tropical forests are cleared (Houghton et al. 2001; Paeth and Hense 2004; Hulme et al. 2001).

Aerosols are found throughout the troposphere, but are most abundant over Africa (Jaenicke 1993; Kaufman and Fraser 1997; Tegen et al. 1996) where they are injected at a rate  $>100$  Tg/year by fires or dust storms during hot windy conditions (Duce 1995). Coarse aerosols (dust) absorb infrared (IR) emissions, warming the lower troposphere (Carlson and Benjamin 1982; Tegen et al. 1996; Ramanathan et al. 2001; Kiehl and Briegleb 1993) and inhibiting convection over the east Atlantic in boreal summer (Hobbs 1993; Lohmann et al. 2000; Jones et al. 2003; Prospero and Lamb 2003; Lohmann and Feichter 2004; Kaufmann et al. 2005).

Aerosol concentrations from anthropogenic biomass burning over tropical Africa (Bird and Cali 1998; Penner et al. 1998; Eck et al. 2001; Stier et al. 2004) create a significant atmospheric burden (Iacobellis et al. 1999; Jacobson 2004). The Amazon and SE Asia are secondary sources. Biomass burning releases GHGs ( $\text{CO}_2$ , CO,  $\text{CH}_4$ ,  $\text{NO}_x$ ) and fine particulates which can be transported some distance in atmospheric layers (Duce 1995). Fine aerosols (mostly black carbon (BC)) absorb ultraviolet (UV) radiation (Langner and Rodhe 1991; Seinfeld and Pandis 1998), whilst GHGs such as tropospheric ozone that absorb IR radiation are photochemically transformed and influence the radiation budget downwind of emission sources (Hobbs 2000). To quantify the radiative fluxes over Africa we need to understand the properties of aerosols. Though observations of scattering can be made, it is difficult to quantify other properties. Radiative forcing of the atmosphere is sensitive to the scattering/extinction ratio of aerosols,  $\omega_o$  (Seinfeld and Pandis 1998); dependent on size distribution, aerosol chemistry and wavelength. Typically  $\omega_o$  is  $>0.6$  for biomass burning aerosols of  $\sim 1$   $\mu\text{m}$  diameter (Anderson et al. 1996; Penner et al. 1998; Haywood et al. 2003). The aerosol optical depth  $\delta$  refers to the fraction of incoming radiation attenuated before reaching the surface (Penner et al. 1994) with typical values from 0.05 in clean air to 1.0 near emission sources such as fires (Seinfeld and Pandis 1998).

Carbonaceous aerosols are produced in biomass burning and are composed of black and organic carbon (BC and OC). BC aerosols are produced during incomplete combustion of moist vegetation (Penner 1995) with a global load of  $\sim 11$  Tg/year in 2000. OC aerosols are contributed from burning of dry vegetation with total emissions of 54 Tg/year. BC is associated with the absorption of solar radiation and heating of the atmosphere, whilst OC is associated with scattering (Penner 1995). Aerosol radiative impacts also depend on cloud level and surface albedo (Kaufman and Fraser 1997; Penner et al. 1998; Keil and Haywood 2003). Earlier studies have estimated the radiative effect of biomass burning aerosols to be rather small (Penner et al. 1992; Anderson et al. 1996; Kaufman and Fraser 1997).

Here we are interested in aerosols and GHGs that absorb radiation and contribute to regional trends in temperature (Andreae and Merlet 2001; Korontzi et al. 2003; Hély et al. 2003). While it is understood that West Africa's climate may be externally forced by variations in sea surface temperature (SST) in the tropical Atlantic (Chang

et al. 2000) with secondary teleconnections to El Niño–Southern Oscillation, here we will focus on localized physical and chemical mechanisms that induce African climate change so that observed trends can be placed into context.

## 2 Data

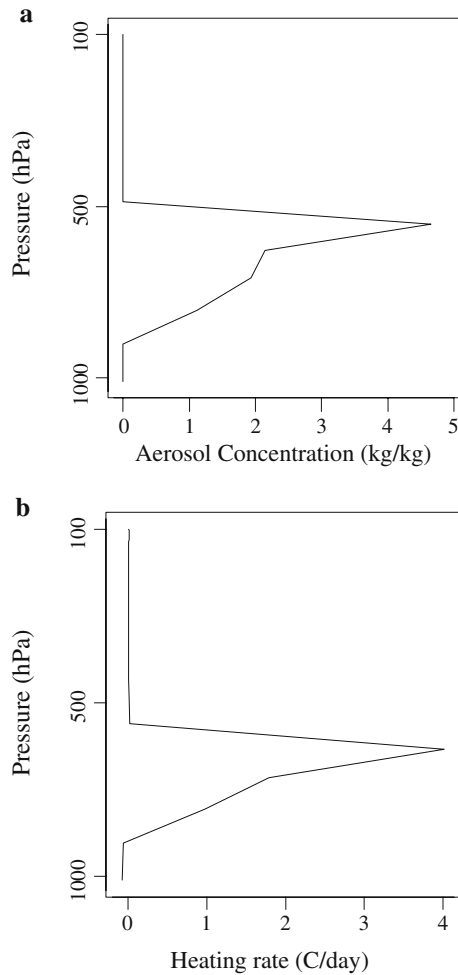
Sun photometers are commonly used to retrieve aerosol optical depth  $\delta$  from sky radiance measurements at wavelengths from 0.340 to 1.020  $\mu\text{m}$  in a narrow field of view at hourly intervals. These instruments form a global network (AERONET) and are calibrated annually at a central lab (NASA Goddard, GSFC). The sun photometer does not determine aerosol type, so properties can be related to anthropogenic or natural sources. From these data the ratio of scattered to absorbed radiation,  $\omega_{500 \mu\text{m}}$  was calculated as 0.88 over northwestern Zambia at the beginning of the biomass burning season, and is comparable with other studies (Anderson et al. 1996; Seinfeld and Pandis 1998; Abel et al. 2003).

Aerosol and atmospheric properties can also be inferred from satellite radiometers such as the Vertical Infrared Scanner (VIRS), Cloud and the Earth's Radiant Energy budget Scanner (CERES) and Advanced Very High Resolution Radiometer (AVHRR). These instruments measure reflected and emitted radiation from the Earth–atmosphere system as well as top of atmosphere (TOA) fluxes and reflectance at different levels. Applying certain threshold criteria, smoke aerosols can be distinguished from clouds, and aerosol optical depth, TOA flux and radiative impacts can be estimated (Kaufman and Fraser 1997; Christopher et al. 2000). Here we extract the satellite remote sensed estimates as described below.

In-situ measurements of aerosol size and concentration have been made using an airborne Passive Cavity Aerosol Spectrometer Probe (PCASP). Other airborne sensors can be used to measure aerosol absorption and response to humidity, aerosol backscatter properties (through the use of lidar), and radiative fluxes at flight level (Penner et al. 1994; Anderson et al. 1996; Haywood et al. 2003). Figure 1a shows the profile concentration observed by airborne PCASP over Zambia in an aged smoke plume. Aerosol concentrations are high in the 800–600 hPa layer (Anderson et al. 1996; Haywood et al. 2003). Profiles reported by Magi and Hobbs (2003) and Hobbs et al. (2003) are also appropriate. The smoke layer contains a mixture of BC, dust and GHGs (Sinha et al. 2003) that is expected to contribute to radiative absorption.

Meteorological data used in this study includes temperature, relative humidity and wind profiles assimilated into the NCEP reanalysis system over Africa at 2.5° resolution from surface stations, and in the east Atlantic from island stations and ships (Kalnay et al. 1996). Upper level air temperatures are assimilated from radiosonde profiles in the period 1949–2006, and since 1976 from satellite radiance profiles. Satellites also provide humidity profiles and cloud drift vectors, whilst aircraft provide reports mainly at cruise level. Linear trends were analyzed at different levels and in various seasons from the CDC website: <http://www.cdc.noaa.gov/Correlation/> for the entire period and for the satellite era, and results were found to be consistent. The seasonal analysis did not reveal much change in temperature trends, as biomass burning peaks in winter when vegetation is dry and dust loading peaks in summer with surface heating—and both can induce radiative warming. In the results

**Fig. 1** **a** Profile of the aerosol concentration for model experiment without cloud, consistent with aircraft profiles reported in Anderson et al. (1996) in aged African smoke plume (size range 0.1–3.0  $\mu\text{m}$ ). **b** The heating profile for simulation without clouds, based on Table 2 specifications



presented below, trends are analyzed as a map at the 700 hPa level and as a vertical north–south section over west Africa for the calendar year. To avoid discontinuities we focus on the satellite era. For this 29 year period, a linear trend correlation value  $>0.4$  is significant at the 98% confidence limit. Radiosonde temperature data at standard levels were extracted at a number of African stations and analyzed for trends over the period 1949–2006, to compare with NCEP reanalysis.

To understand the physical processes underlying temperature changes over west Africa, NCEP reanalysis vertical motion ( $\omega$ ) data were analyzed for trends. To determine whether changes in atmospheric composition may be a source of regional climate change, aerosol optical depth or thickness (AOT) was extracted from NASA TOMS satellite data via the IRI website: <http://iridl.ldeo.columbia.edu/SOURCES/.NASA/.GSFC/.TOMS/>. To objectively map the plumes emanating from Africa, a singular value decomposition (SVD) analysis was performed. This involves an eigenvector decomposition of the covariance matrix for

successive monthly AOT fields, such that the variability is reduced to modes in order of decreasing explained variance normalized to a total of one. For each unique mode there is a spatial pattern of weights or loadings and a series of expansion coefficients or time scores that describe its temporal fluctuations, both with units of standard deviations relative to each mode. From the SVD analysis two distinct modes are found: mode-1 explaining 34% of the total variance is the Sahel dust plume, while mode-2 accounting for 13% of the variance is the Congo smoke plume. The mean seasonal cycle and trends of AOT were calculated over these two regions and compared with satellite estimated ozone ( $O_3$ ) data from Ziemke et al. (2005) [http://code916.gsfc.nasa.gov/Data\\_services/cloud\\_slice/](http://code916.gsfc.nasa.gov/Data_services/cloud_slice/). Recent AIRS satellite images were evaluated to identify CO concentrations in the 700 hPa layer from: [http://mopitt.eos.ucar.edu/mopitt/data/plots/mapsv3\\_mon.html](http://mopitt.eos.ucar.edu/mopitt/data/plots/mapsv3_mon.html). In addition, satellite–gauge merged GPCC rainfall and NASA vegetation (NDVI) data were extracted from the IRI website for comparison with co-located 700 hPa temperature, AOT and  $O_3$  data. Cross-correlations were computed between the smoothed monthly time series. The degrees of freedom is  $\sim 60$ , so correlations  $>|0.25|$  are significant at the 95% confidence limit. Values pertain to the 1980–2005 period, notwithstanding the TOMS satellite data gap in 1994–1995.

Estimated future trends of temperature in the elevated layer over Africa were extracted from GFDL C2.1 model forecasts using the A1B scenario prepared for the IPCC/AR4 via <http://iridl.ldeo.columbia.edu/SOURCES/WCRP/CMIP3/>. A number of authors have evaluated the various IPCC/AR4 GCM projections and found the GFDL C2.1 to be consistent with the ensemble average and to well represent climate variability (Meehl et al. 2007). Comparisons were made between the radiosonde and GCM trends of 700 hPa temperature for Dakar and Brazzaville; and between observed and model trends of temperature and rainfall, using gridded data over the period 1950–2005. Model data were adjusted to the observations in the overlapping period, and both past and future time series were smoothed with a 5 year running mean and analyzed for trends. Temperature data were analyzed for distribution and a  $r^2$  value of 0.80 with respect to a second order Gaussian fit was deemed to be sufficiently normal to make use of standard tests for significance.

### 3 Results

#### 3.1 Simulation of heating by aerosols and GHGs

We conceptualize radiation absorption by aerosols with the equation of Haywood and Shine (1995) where  $\Delta F$  varies with  $\omega_0$ . All terms are defined in Table 1:

$$\Delta F = -DS_0\beta\omega_{0\lambda=0.500\ \mu\text{m}}\tau_i^2 \left[ (1 - \alpha_s)^2 - \frac{2\alpha_s}{\beta} \left( \frac{1}{\omega_{0\lambda=0.500\ \mu\text{m}}} - 1 \right) \right] \quad (1)$$

The net radiative absorption by dust and biomass burning aerosols based on values in Table 1 is consistent with that found by Ichoku et al. (2003) and Keil and Haywood (2003) i.e.  $-15$  to  $-24\ \text{W m}^{-2}$  compared to our  $-29\ \text{W m}^{-2}$ , computed as the difference of  $\Delta F$  between top of the atmosphere and surface (a negative value indicates absorption). Although we have a useful result, it does not provide information on the vertical distribution of radiative absorption that is critical to our

**Table 1** Parameters (adapted from Anderson et al. 1996) to estimate radiative flux

Parameter	Value	Meaning
D	0.46	Day length
$S_0$ ( $\text{W m}^{-2}$ )	1,370	Solar constant
$\beta$	0.18	Upscatter fraction
$\omega_0$	0.88	Single scattering albedo
$\delta_a$	0.37	Aerosol optical depth
$\alpha_s$	0.20	Surface reflectance
$\tau_i^2$	0.76	Atmospheric transmittance
$\Delta F$ ( $\text{W m}^{-2}$ )	-29	Tropospheric absorption

Units are dimensionless fractions unless specified

understanding. It is averaged over the troposphere, and could involve surpluses and deficits in various layers.

A second approach is to use a simplified radiative transfer model (Edwards and Slingo 1996), focusing on shortwave radiation absorption by aerosols using tropical profiles. The model requires absorption and scattering coefficients (from aerosol size distribution), the scattering albedo and asymmetry factor. Here we adopt a profile (Fig. 1a) based on a number of sources: SAFARI aircraft measurements (Anderson et al. 1996; Haywood et al. 2003), ozone profiles from commercial aircraft (Mfuamba 2007) and aerosol concentrations from Calipso satellite lidar sections via website: <http://www-calipso.larc.nasa.gov/products/>. The model estimates net irradiances and corresponding heating rates (Table 2) for each atmospheric layer, depending on:

$$\delta_a = Mk_{ext} \frac{\partial p}{g} \quad (2)$$

where  $g$  is gravity and  $\partial p$  indicates the aerosol layer depth, where  $p$  is pressure (Pa). The values used for Africa are:  $\delta_a = 0.5$ ,  $\rho = 1.25 \text{ kg m}^{-3}$ ,  $k_{ext} = 8.37 \cdot 10^3 \text{ m}^2 \text{ kg}^{-1}$ , assuming an albedo for dry savanna of 0.2. The atmospheric mass  $M$  adjusts to maintain  $\delta_a$  constant over an aerosol layer in accordance with observations. The first simulation without clouds (African dry season) is contrasted with the second simulation with clouds below the smoke layer approximating conditions over the tropical east Atlantic, and the third simulation with clouds above the smoke layer as would be expected in summer.

We calculate a  $\Delta F$  of  $\sim -60 \text{ W m}^{-2}$  (Table 2) compared to  $\sim -30 \text{ W m}^{-2}$  from Anderson et al. (1996), Penner et al. (1998), Keil and Haywood (2003). Airborne measurements in the burning season have found values up to  $-100 \text{ W m}^{-2}$  yielding a heating  $\sim 5^\circ\text{C}$  (Pilewski et al. 2003). Our calculated heating profile in cloudless conditions shows a  $3^\circ\text{C}$  temperature increase within the aerosol layer (Fig. 1b) in agreement with Hsu et al. (2003). This heating strengthens the inversion at the top of

**Table 2** Specifications and results for simulations of radiative forcing, divided into TOA (referring to the upward longwave component) and SFC (downward shortwave part)

Simulation	Aerosol layer (hPa)	Cloud layer (hPa)	$\Delta F_{\text{toa}}$ ( $\text{W m}^{-2}$ )	$\Delta F_{\text{sfc}}$ ( $\text{W m}^{-2}$ )
1	600–850	None	-6.1	-67.1
2	590–750	850–950	+18.5	-60.1
3	590–850	450–520	-6.5	-66

Negative values indicate absorption

the boundary layer. In simulation 2 and 3, the radiative effect is calculated for cloudy skies above and below the aerosol layer. The  $\Delta F$  increases from  $-59.5$  to  $-78.6$   $\text{W m}^{-2}$  implying additional heating when shallow stratus clouds underlie the aerosol layer, in agreement with Keil and Haywood (2003) and Myhre et al. (2003) over the east Atlantic. Although smoke plumes mix in cloud layers over the Atlantic, the bulk of aerosols are thought to remain beneath (Anderson et al. 1996; Li et al. 1998; Keil and Haywood 2003). In simulation 3 where the cloud overlies the aerosol layer, the  $\Delta F$  and heating rate is similar to dry season conditions (Table 2). Considering the radiation absorbed at the top of atmosphere ( $\Delta F_{\text{TOA}}$ ) and surface ( $\Delta F_{\text{SFC}}$ ) we are able to distinguish impacts on the upward longwave flux and downward shortwave flux. Most absorption is in the downward shortwave component ( $< -60$   $\text{W m}^{-2}$ ). In comparison the upward longwave absorption is about 10% of the total.

### 3.2 Aerosol optical thickness climatology

To highlight the extent of Africa's influence on atmospheric composition, SVD loading maps and time scores for AOT are given in Fig. 2. The leading pattern reveals a broad plume extending across the southern Sahara desert and west African Sahel, into the east Atlantic (Fig. 2a). It is most dense in the  $10$ – $20^\circ\text{N}$ ,  $20^\circ\text{W}$ – $10^\circ\text{E}$  zone around Dakar, Senegal where AOT values regularly exceed 1, then decline into the east Atlantic with deposition and entrainment taking place. The northern 'dust' plume is prevalent in May–July season when surface heating and winds are strongest (Fig. 3a). Mode-2 is comprised of a southern 'smoke' plume (Fig. 2b) which extends west of the Congo Basin across the Gulf of Guinea ( $10^\circ\text{S}$ – $5^\circ\text{N}$ ,  $20^\circ\text{W}$ – $10^\circ\text{E}$ ).

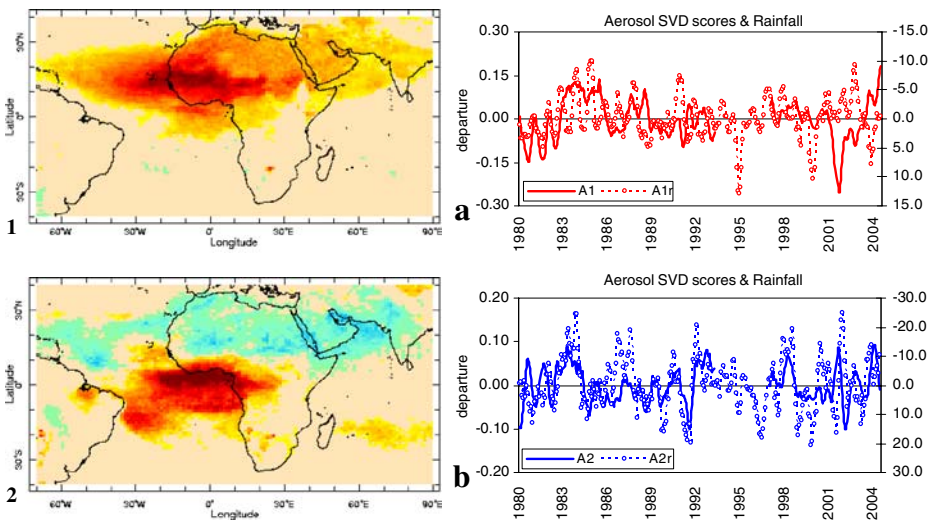
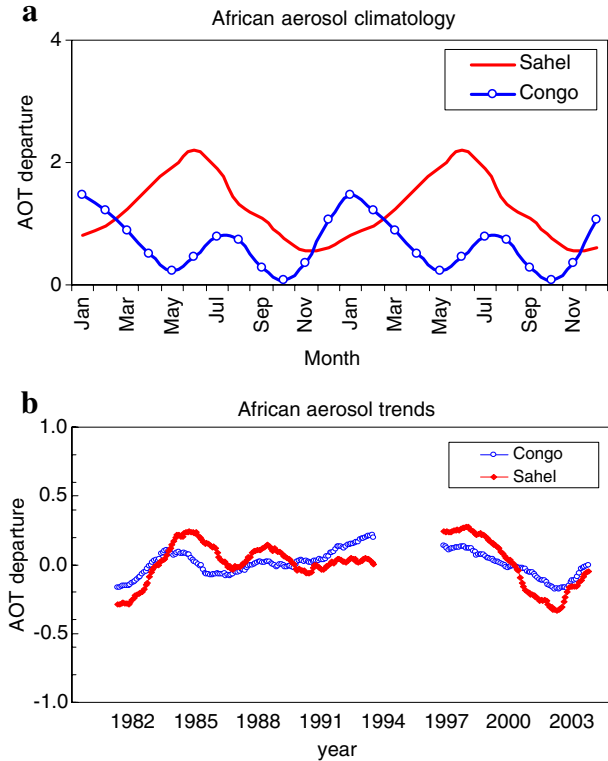


**Fig. 2** SVD analysis of AOT over the period 1980–2005. Loading maps for mode 1 (a) and mode 2 (b) and their respective time scores compared with (inverted) rainfall in co-located (red-shaded) zones. Loading maps are contoured from  $-3$  to  $+3$  sigma (blue–neutral–red); time scores were computed with a 5-month running mean. White dots indicate positions of Dakar (a) and Brazzaville (b)

**Fig. 3** **a** Seasonal cycle  $\times 2$  of AOT in the Sahel and Congo plumes based on SVD analysis of TOMS satellite data in the period 1980–2005. **b** Smoothed AOT anomalies averaged over the Sahel and Congo plumes



Its seasonal cycle is bimodal with a main peak in January–February and a minor peak in July–August (Fig. 3a). The time scores for the northern and southern plumes exhibit both seasonal and inter-annual variability that is inversely related to rainfall ( $r = -0.29$  to  $-0.49$ , respectively). As expected, lower rainfall promotes the release of dust and biomass burning. SVD analysis provides an orthogonal view of AOT, however when time series are extracted for the Sahel and Congo plumes, they are found to be significantly correlated at  $+0.61$ . Smoothed temporal variations of AOT in the northern and southern plumes are shown in Fig. 3b. There is a rising trend in the 1980s that reverses in the mid-1990s when rainfall and vegetation increased. According to data analyzed from the NASA website, tropospheric  $O_3$  values are greatest in the southern plume, averaging 35–40 ppb. Values are  $\sim 10\%$  less in the northern plume. Tropospheric  $O_3$  values peak in the winter biomass burning season, alternating from north (December to February) to south (June to August) and can exceed 150 ppb in the 2–4 km layer over tropical west Africa and the east Atlantic at times (Mfuamba 2007; Hawkins et al. 2007). NASA MOPITT images from the AIRS satellite radiometer indicate that monthly mean carbon monoxide concentrations in the 700 hPa layer exceed 200 ppb in the southern smoke plume, with peak values oscillating north–south similar to  $O_3$ .

### 3.3 Effect of aerosols on clouds

There are indirect effects of aerosols: increased cloud optical thickness and albedo (Twomey 1977), and reduced coalescence efficiency (Rotstajn and Penner 2001). The applicable equation is:

$$\Delta F = F_d \tau_a^2 f_c \Delta \alpha_p \tag{3}$$

where  $F_d$  is the average downward flux at the top of the atmosphere,  $\tau_a$  is atmospheric transmission above the cloud layer,  $f_c$  is fractional cloud cover and  $\Delta \alpha_p$  is the change in cloud albedo  $\alpha_c$  (Lacis and Hansen 1974). Cloud optical depth  $\delta_c$  can be calculated from: (Twomey 1977):

$$\delta_c = h \left( \frac{9\pi LWC^2 N_d}{2\rho^2} \right)^{\frac{1}{3}} \tag{4}$$

where  $h$  is the cloud layer thickness,  $LWC$  is the liquid-water content within the cloud layer,  $N_d$  is the cloud droplet concentration and  $\rho$  is water density. We use biomass burning aerosol concentrations, and the dry savanna albedo adopted earlier. All other parameters are consistent with biomass burning conditions except we use a global value for fractional cloud cover.

The parameters and calculated values used in Eqs. 4 and 5 are given in Table 3, with some taken from the literature. Our estimate is  $-8.4 \text{ W m}^{-2}$  indicating some radiative absorption by clouds similar to Ichoku et al. (2003)  $-10 \text{ W m}^{-2}$ , but above that of Kaufman and Fraser (1997) for the Amazon Basin ( $-2 \text{ W m}^{-2}$ ). The second indirect effect of aerosols is to reduce coalescence efficiency (Rosenfeld 1999), so

**Table 3** Values used to calculate the indirect effect of biomass burning aerosols

Parameter	Input value	Calculated
$F_d \text{ (W m}^{-2}\text{)}$	1,370	
$\tau_a$	0.92	
$f_c$	0.24	
$\Delta \alpha_p$		0.09
$\alpha_s$	0.20	
$\alpha_c$		0.61
$\alpha_c'$		0.49
$\alpha_p$		0.64
$\alpha_p'$		0.55
$\delta_c$		12.06
$\delta_c'$		7.47
$H \text{ (m)}$	280	
$LWC \text{ (g m}^{-3}\text{)}$	0.29	
$P \text{ (g m}^{-3}\text{)}$	$1.25 \times 10^3$	
$N_d \text{ (cm}^{-3}\text{)}$	1,800	
$N_d' \text{ (cm}^{-3}\text{)}$	1,000	
$\Delta F \text{ (W m}^{-2}\text{)}$		-8.4

Primed values indicate background conditions. Further information is contained in Whitehall (2003). Units are dimensionless unless specified

clouds holding water vapor resist precipitating (Rotstayn and Penner 2001). This aerosol effect was studied by Lohmann et al. (2000) and a forcing of  $-1.5 \text{ Wm}^{-2}$  was determined. The second indirect effect limits the release of latent heat in the tropics (James 1995), modulating the Hadley circulation and tropical convection (Jury and Winter 2009). In summary, the indirect effect is  $\sim 10\%$  of the direct effect, and both contribute to warmer and drier conditions with less efficient rainfall production.

### 3.4 Analysis of warming trends

In Fig. 4a the linear trend correlation map for 700 hPa temperatures illustrates significant warming near the top of the boundary layer. The area of significant positive trend displays two broad zonal axes along  $10^\circ\text{S}$  from  $30^\circ\text{E}$  to  $20^\circ\text{W}$  (Zambia to Ascension), and along  $10^\circ\text{N}$  from  $40^\circ\text{E}$  to  $50^\circ\text{W}$  (Ethiopia to Barbados). The area of maximum warming coincides with areas of dense aerosol loading (Fig. 2a, b) and high concentrations of GHGs such as  $\text{CO}$  and  $\text{O}_3$ .

Past trends in 700 hPa temperature anomalies based on radiosonde data at Brazzaville and Dakar are analyzed in Fig. 4b. The linear trends are nearly identical,  $+0.85^\circ\text{C}$  over the period 1950–2005. However the  $r^2$  fit of the trend is greater for Brazzaville (0.77) compared to Dakar (0.56), suggesting that inter-decadal variability is high within the northern dust plume. Brazzaville is located within the southern smoke plume and is affected by recirculation (surface equatorial westerly winds undercutting the deep easterly flow). These factors could explain its more consistent upward trend of  $\sim 0.015^\circ\text{C}/\text{year}$ . The correlation between 700 hPa temperature and AOT over the period 1980–2005 is  $+0.18$ . This fails to achieve statistical significance given 60 degrees of freedom, probably due to the upward trend in temperature. Thus the smoke and dust plumes may concentrate radiative absorption at the top of the boundary layer, but aerosols alone are unlikely to be the cause of warming trends in the elevated layer.

GFDL C2.1 model projected 700 hPa temperature trends are shown in Fig. 4b for the SRES A1B scenario. Temperatures increase as a second order polynomial, reaching  $+2^\circ\text{C}$  by 2050 in the elevated layer over Dakar and almost  $+3^\circ\text{C}$  at Brazzaville. Trends are significant at the 99% confidence limit, after deflating the degrees of freedom for smoothing and considering standardized values.

In Fig. 5a, west African temperature trends are analyzed as a vertical cross section  $25^\circ\text{S}$ – $30^\circ\text{N}$ , 925–500 hPa based on NCEP re-analysis data averaged over west African longitudes ( $0$ – $30^\circ\text{E}$ ) in the period 1976–2005. Significant upward temperature trends are noted in the 700 hPa layer, extending symmetrically from  $20^\circ\text{S}$  to  $20^\circ\text{N}$ . Maximum warming occurs over the Congo Basin ( $2^\circ\text{S}$ – $7^\circ\text{N}$ ) in the 925–850 hPa layer. Our heating profile (Fig. 1b) anticipated most of the warming at the top of the aerosol layer from absorption of incoming UV radiation. However temperature trends indicate that heating extends into the lower aerosol layer, pointing to absorption of outgoing IR radiation that depends on surface temperatures, albedo and land use. The impact of aerosols on relative humidity trends is shown in Fig. 5b. Atmospheric moisture displays a faster decline north of the equator, than south. The dry zone extends from  $2^\circ\text{S}$  to  $15^\circ\text{N}$  and vertically from 925 to 700 hPa, with an axis along  $10^\circ\text{N}$ . We postulate that higher GHG concentrations in the southern smoke plume (Fig. 2b) induce warming without drying, whilst the northern dust plume over the Sahel (Fig. 2a) induces both warming and drying. The external influence of

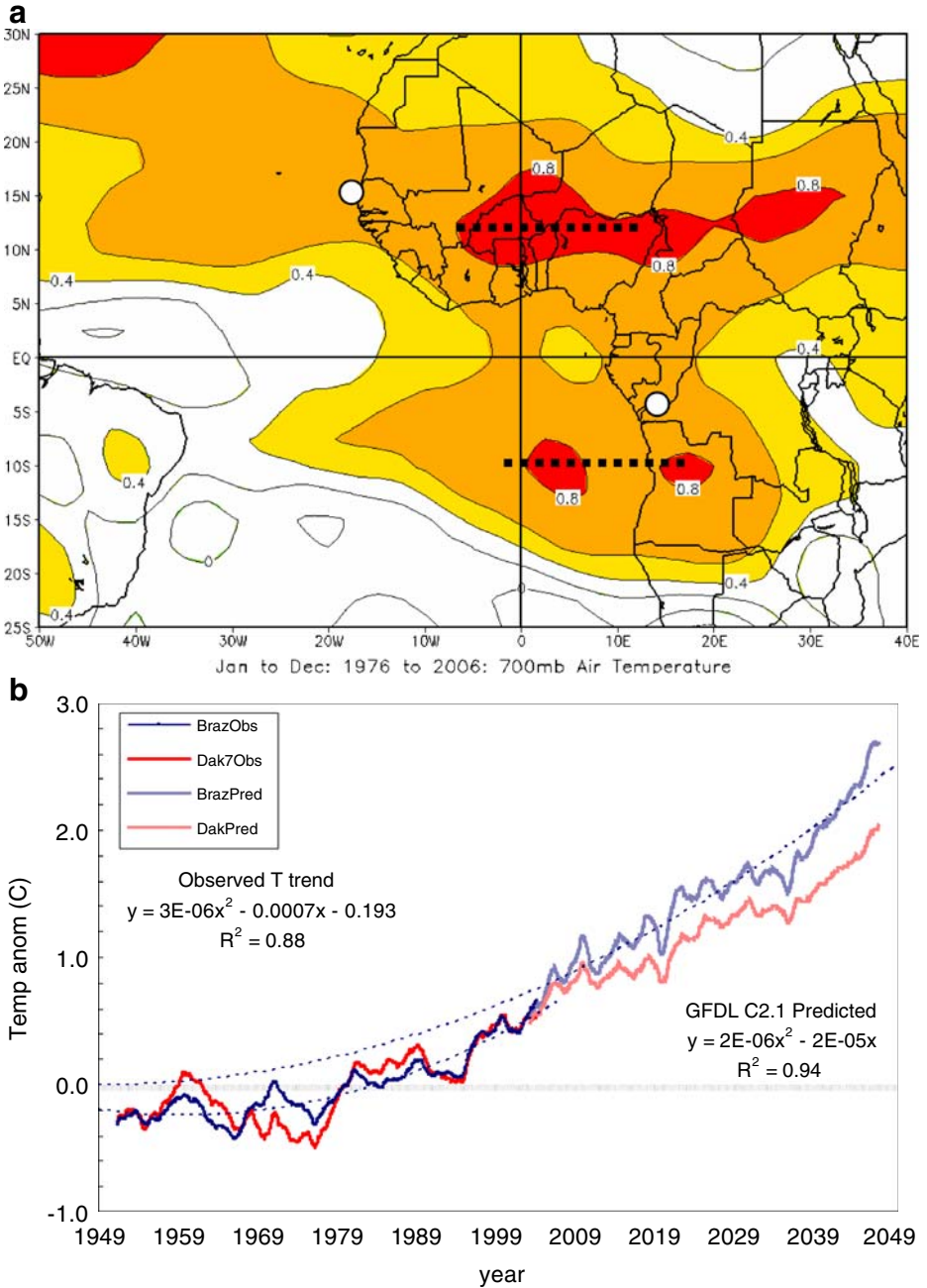


**Fig. 4** **a** Linear trend correlations for 700 hPa temperature in the satellite era. Areas  $r > 0.4$  are shaded and statistically significant; dots refer to station positions. **b** Radiosonde-observed (1950–2006) and GFDL-predicted (2001–2049) 700 hPa temperatures for Brazzaville (blue) and Dakar (red), smoothed with a 5-year running mean, with  $r^2$  fit for polynomial trend

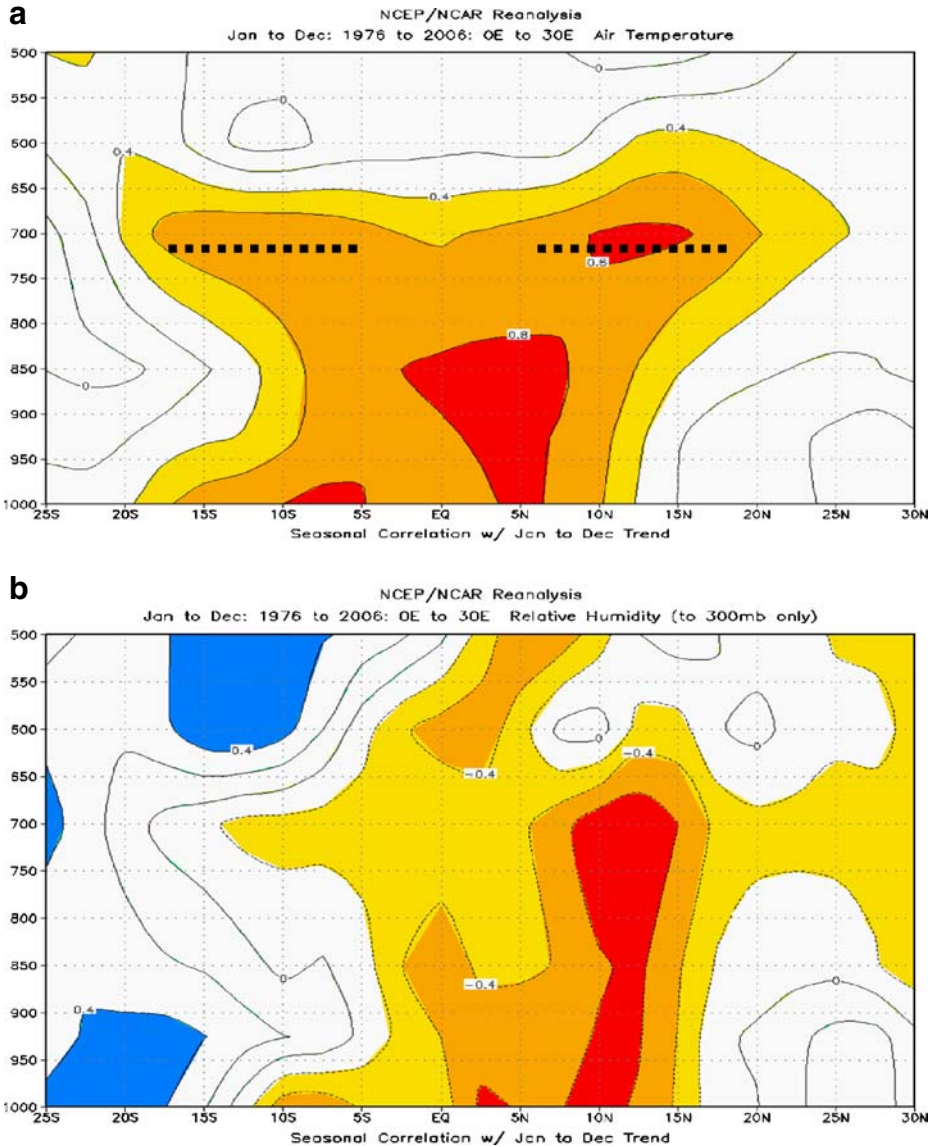


**Fig. 5** Linear trend correlations for temperature (a) and humidity (b) averaged over the 0–30°E longitudes, plotted as a vertical section from the surface to 5.5 km (500 hPa). The *dashed line* highlights warming at the top of the aerosol layer

multi-decadal fluctuations of Atlantic SSTs on vertical motion and moisture advection may also play a role in the humidity trend. These drying trends translate into declining rainfall as evident in Fig. 6 in both past observed and future GFDL model projected data for Dakar and Brazzaville. Further work on the indirect effects of aerosols on clouds is necessary to provide conclusive results.

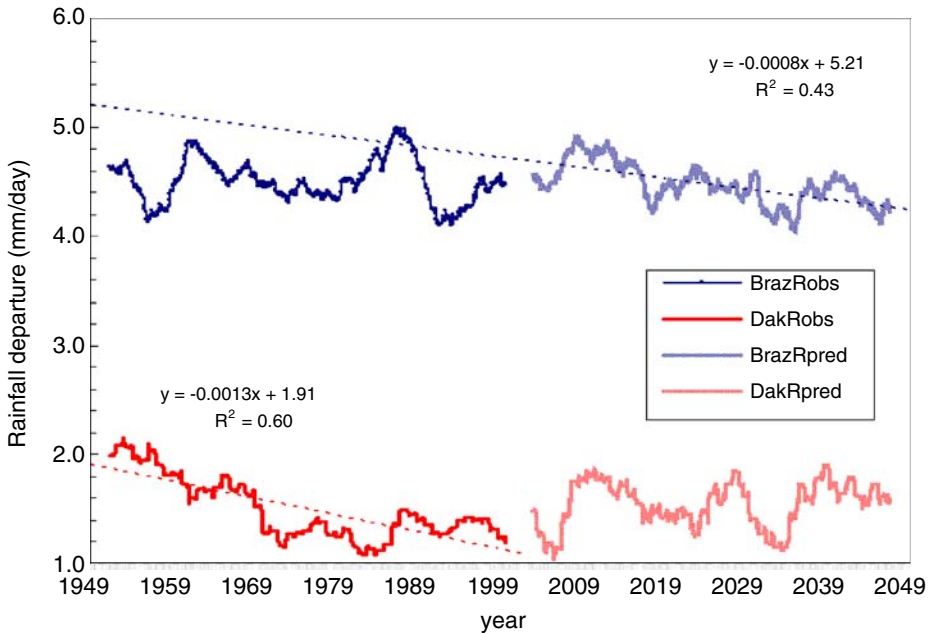


**Fig. 6** Observed and predicted rainfall trends in the vicinity of Dakar and Brazzaville, based on CRU gridded rainfall data and the GFDL C2.1 A1B projection, smoothed with a 5-year running mean

#### 4 Discussion

The aerosol plumes of Africa provide  $\sim 100$  Tg of total mass output each year, much of it advected westward toward the tropical Atlantic, where deposition of particles and transformation of gases occurs. The Saharan desert ejects dust into the northern subtropics mainly during summer (Fig. 3a) which reflects and scatters radiation in the 2–4 km layer (Wong et al. 2007), and later absorbs radiation following deposition. Although dust emissions vary seasonally depending on surface conditions such as rainfall, vegetation cover and heat flux, little inter-decadal trend was evident (cf. Fig. 3b) that could contribute to observed increases of 700 hPa layer temperatures. The amount of biomass that is burned is related to land use and population density on the margins of the African savanna. Most African vegetation fires occur in the  $15^{\circ}\text{S}$ – $10^{\circ}\text{N}$  latitude band (Anyamba et al. 2003). There, population has doubled between 1975 and 2000. The emissions are composed of aerosols and GHGs (Sinha et al. 2003) that absorb radiation, and some GHGs such as tropospheric  $\text{O}_3$  and CO are short-lived ( $\sim 10$  days, Hobbs 2000; Houghton et al. 2001) and can therefore contribute to regional differences in greenhouse warming. Tropospheric ozone levels have risen from 36 to 39 ppb or  $\sim 8\%$  over west Africa and the east Atlantic during the period 1980–2005, based on NASA data. However cross-correlations between  $\text{O}_3$  and 700 hPa temperatures are inconclusive.

Aircraft measurements of radiative fluxes above and below the African smoke layer have been made (Bergstrom et al. 2003) and a net radiative flux  $\sim -20$   $\text{W m}^{-2}$  has been determined, in agreement with our simulations for cloudless condi-

tions (direct effect). There may be more aerosol-induced radiative absorption over northwest Africa and more GHG-induced absorption over southwest Africa and the Gulf of Guinea, but upward trends of 700 hPa air temperature show little distinction (Fig. 4a). The vertical section (Fig. 5a) reveals warming in the aerosol layer over the Congo, pointing to absorption by GHGs. In the equatorial zone low level westerlies may re-circulate the photochemically transformed air. Ozone levels at Brazzaville exceed 80 ppb in the 2–3 km layer according to MOZAIC data (Mfuamba 2007).

In our attribution budget we employ the thermodynamic equation:

$$\partial T_{700}/\partial t = (\kappa T/p) W + 1/g C_p (\partial F/\partial p) \quad (5)$$

with terms for vertical motion ( $W$ ) and radiative heating quantifying the change of temperature  $T$  with time  $t$ . Horizontal temperature advection is assumed to be negligible in the tropics. Trends of sinking motion in the 4–6 km layer over west Africa are  $<10^{-3} \text{ m s}^{-1}$  yielding  $\Delta T \sim 5 \times 10^{-3} \text{ C/year}$ . So the physical contribution is relatively small over Africa.

The internal heating rate is estimated from  $1/g C_p (-\partial F/\partial p)$ , where  $g$  is gravity,  $C_p$  is the specific heat capacity of air, and  $\partial F$  is the net radiative flux ( $\Delta F$ , negative value refers to absorption) across the layer  $\partial p$  (Hobbs 2000; Pilewski et al. 2003). The layer thickness varies with season and latitude, but is taken as extending from 1.5 to 4 km based on aircraft and satellite lidar data, a  $\partial p$  of  $\sim 250$  hPa consistent with simulation 1 above. If we assume a mean annual condition (neglecting seasonal migration) and consider tropical west Africa ( $10^\circ\text{S}$ – $10^\circ\text{N}$ ), a fractional absorption of  $\sim 2\%$  ( $-20 \text{ W m}^{-2}$ ) over a volume  $4 \times 10^9 \text{ m}^3$ , then a greenhouse induced warming  $\Delta T$  of  $\sim 10^{-2} \text{ C/year}$  is found, accounting for most of the observed trend at 700 hPa (cf. Fig. 4b). This atmospheric warming spreads over broad areas and occurs in all seasons, so radiative impact does not appear to be that sensitive to albedo or clouds.

Warming of the 850–600 hPa layer reduces convective available potential energy (CAPE) as shown by Wong et al. (2007). A more stable atmosphere inhibits rainfall (cf. Fig. 6), contributing to diminishing streamflow (Jury 2003) that puts the continent's water resources at risk. The African climate is changing and there is evidence of a regional footprint that extends into the tropical east Atlantic.

## References

- Abel SJ, Haywood JM, Highwood EJ, Li J, Buseck PR (2003) Evolution of biomass burning aerosol properties from an agriculture fire in southern Africa. *Geophys Res Lett* 30:1783. doi:10.1029/2003GL017342
- Anderson BE, William GB, Gerald GL, Edward BV, Collins JE, Glen SW, Bagwell DR, Hudgins CH, Blake DR, Blake NJ (1996) Aerosols from biomass burning over the tropical South Atlantic region: distribution and impacts. *J Geophys Res* 101:24117–24137
- Andreae MO, Merlet P (2001) Emission of trace gases and aerosols from biomass burning. *Glob Biogeochem Cycles* 15:955–966
- Anyamba A, Justice CO, Tucker CJ, Mahoney R (2003) Seasonal to interannual variability of vegetation and fires at SAFARI-2000 sites inferred from AVHRR time series data. *J Geophys Res* 108(D13):8507
- Bergstrom RW, Pilewskie P, Schmid B, Russell B (2003) Estimates of spectral aerosol single scattering albedo and aerosol radiative effects during Safari2000. *J Geophys Res* 108(13):8474
- Bird MI, Cali JA (1998) A million-year record of fire in sub-Saharan Africa. *Nature* 394:767–769

- Carlson T, Benjamin S (1982) Radiative heating rates for desert aerosol. In: Deepak A (ed) *Atmospheric aerosols: their formation, optical properties and effects*. Spectrum, Hampton, pp 435–457
- Chang P, Saravanan R, Ji L, Hegerl GC (2000) The effect of local sea surface temperature on atmospheric circulation over the tropical Atlantic sector. *J Climate* 13:2195–2216
- Christopher SA, Joyce C, Zhang J, Li X, Todd A (2000) Shortwave direct radiative forcing of biomass burning aerosols estimated using VIRS and CERES data. *Geophys Res Lett* 27:2197–2200
- Duce RA (1995) Sources, distributions, and fluxes of mineral aerosols and their relationship to climate. In: Charlson RJ, Heintzenburg J (eds) *Aerosol forcing of climate*. Wiley, New York, pp 43–72
- Eck TF, Holben BN, Ward DE, Dubovik O, Reid JS, Smirnov A, Mukelabai MM, Hsu NC, O'Neill NT, Slutsker I (2001) Characterization of the optical properties of biomass burning aerosols in Zambia during the 1997 ZIBBEE field campaign. *J Geophys Res* 106:3425–3448
- Edwards JM, Slingo A (1996) Studies with a flexible new radiation code: I: choosing a configuration for a large-scale model. *Q J R Meteorol Soc* 122:689–719
- Feddema JJ, Freire S (2001) Soil degradation, global warming and climate impacts. *Clim Res* 17:209–216
- Hawkins MD, Morris VR, Nalli NR, Joseph E (2007) Comparison of aerosol and ozone profiles within Saharan dust and biomass burning plumes. *Proc. AMS Conf. Atmos. Chem, Austin, J7.9*
- Haywood JM, Shine KP (1995) The effect of anthropogenic sulphate and soot aerosol on the clear sky planetary radiation budget. *Geophys Res Lett* 22:603–606
- Haywood J, Francis P, Dubovik O, Glew MD, Holben BN (2003) Comparison of aerosol size distributions, radiative properties and optical depths determined by aircraft observations and sun photometers during SAFARI-2000. *J Geophys Res* 108(D13):SAF7.1–SAF7.12
- Hély C, Alleaume S, Swap RJ, Shugart HH, Justice CO (2003) SAFARI-2000 characterization of fuels, fire behaviours, combustion completeness, and emissions from experimental burns in infertile grass savannas in western Zambia. *J Arid Environ* 54:381–394
- Hobbs PV (1993) Aerosol–cloud interactions. In: Hobbs PV (ed) *Aerosol–cloud–climate interactions*. Academic, New York, pp 33–95
- Hobbs PV (2000) *Introduction to atmospheric chemistry*. Cambridge University Press, New York
- Hobbs PV, Sinha P, Yokelson RJ, Christian TJ, Blake DR, Gao S, Kirchstetter TW, Novakov T, Pilewskie P (2003) Evolution of gases and particles from a Savanna fire in South Africa. *J Geophys Res* 108(D13):8485. doi:10.1029/2002JD002352
- Houghton JT, Ding Y, Griggs DJ, Noguer M, Van der Linden PJ, Dai X, Maskell K, Johnson CA (eds) (2001) *Climate change. The Scientific basis*, Cambridge
- Hsu NC, Herman JR, Tsay S (2003) Radiative impacts from biomass burning in the presence of clouds during boreal spring in southeast Asia. *Geophys Res Lett* 30(4):1224
- Hulme M, Doherty R, Ngara T, New M, Lister D (2001) African climate change: 1900–2100. *Clim Res* 17:145–168
- Iacobellis SF, Frouin R, Somerville RCJ (1999) Direct climate forcing by biomass-burning aerosols: impact of correlations between controlling variables. *J Geophys Res* 104:12031–12045
- Ichoku C, Remer LA, Kaufman YJ, Levy R, Chu DA, Tanre D, Holben BN (2003) MODIS observation of aerosols and estimation of aerosol radiative forcing over southern Africa during Safari2000. *J Geophys Res* 108(D13):8499
- Jacobson MZ (2004) The short-term cooling but long-term warming due to biomass burning. *J Climate* 17:2909–2926
- Jaenicke R (1993) Tropospheric aerosols. In: Hobbs PV (ed) *Aerosol–cloud–climate interactions*. Academic, New York, pp 1–131
- James IN (1995) *Introduction to circulating atmospheres*. Cambridge University Press, Cambridge
- Jones C, Mahowald N, Luo C (2003) The role of Easterly Waves on African desert dust transport. *J Climate* 16:3617–3628
- Jury MR (2003) Coherent variability of African River flows, composite climate structure and the Atlantic circulation. *Water SA* 29:1–10
- Jury MR, Winter A (2009) Warming of an elevated layer over the Caribbean. *Clim Change*. doi:10.1007/s10584-009-9658-3
- Kalnay E, co-authors (1996) The NCEP/NCAR 40-year reanalysis project. *Bull Am Meteorol Soc* 77:437–471
- Kaufman YJ, Fraser RS (1997) The effect of smoke particles on clouds and climate forcing. *Science* 277:1636–1639

- Kaufmann YJ, Koren I, Remer LA, Tanre D, Ginoux P, Fan S (2005) Dust transport and deposition observed from MODIS over the Atlantic Ocean. *J Geophys Res* 110(10):512
- Keil A, Haywood JM (2003) Solar radiative forcing by biomass burning aerosol particles in cloudy skies during SAFARI-2000. *J Geophys Res* 108(D13):8467
- Kiehl JT, Briegleb BP (1993) The relative roles of sulfate aerosols and greenhouse gases in climate forcing. *Science* 260:311–314
- Korontzi S, Justice CO, Scholes RJ (2003) Influence of timing and spatial extent of savanna fires in southern Africa on atmospheric emissions. *J Arid Environ* 54:395–404
- Lacis AA, Hansen JE (1974) A parameterization for the absorption of solar radiation in the earth's atmosphere. *J Atmos Sci* 31:118–133
- Langner J, Rodhe H (1991) A global-three-dimensional model of the tropospheric sulfur cycle. *J Atmos Chem* 13:225–263
- Li Z, Williams AL, Rood MJ (1998) Influence of soluble surfactant properties on the activation of aerosol particles containing inorganic solute. *J Atmos Sci* 55:1859–1866
- Lohmann U, Feichter J (2004) Global indirect aerosol effects: a review. *Atmos Chem Phys Discuss* 4:7561–7614
- Lohmann U, Feichter J, Penner J, Leaitch R (2000) Indirect effect of sulfate and carbonaceous aerosols: a mechanistic treatment. *J Geophys Res* 105:12193–12206
- Magi BI, Hobbs PV (2003) Effects of humidity on aerosols in southern Africa during the biomass burning season. *J Geophys Res* 108(D13):SAF31.1–SAF31.12
- Meehl GA, Covey C, Delworth T, Latif M, McAvaney B, Mitchell JFB, Stouffer RJ, Taylor KE (2007) The WCRP CMIP3 multimodel dataset: a new era in climate change research. *Bull Am Meteorol Soc* 88:1383–1394
- Mfuamba J-P (2007) Tropospheric ozone climatology at Brazzaville. M.Sc. thesis, Univ. K.Z. Natal, Durban, 88 pp
- Myhre G, Bertsens TK, Haywood JM, Sundet JK, Holben BN, Johnsrud M, Stordal F (2003) Modeling the solar radiative impact of aerosols from biomass burning during SAFARI-2000. *J Geophys Res* 108(D13):8501
- Paeth H (2004) Key factors in African climate change evaluated by a regional climate model. *Erdkunde* 58:290–315
- Paeth H, Hense A (2004) SST versus climate change signals in West African rainfall: 20th century variations and future projections. *Clim Change* 65:179–208
- Penner JE (1995) Carbonaceous aerosols influencing atmospheric radiation: black and organic carbon. In: Charlson RJ, Heintzenburg J (eds) *Aerosol forcing of climate*. Wiley, New York, pp 91–108
- Penner JE, Dickson RE, O'Neill CA (1992) Effects of aerosols from biomass burning on the global radiation budget. *Science* 256:1432–1433
- Penner JE, Charlson RJ, Hales JM, Laulainen NS, Leifer R, Novalov T, Ogren J, Radke LF, Schwartz SE, Travis L (1994) Quantifying and minimizing uncertainty of climate forcing by anthropogenic aerosols. *Bull Am Meteorol Soc* 75:375–400
- Penner JE, Chuang CC, Grant K (1998) Climate forcing by carbonaceous and sulfate aerosols. *Clim Dyn* 14:839–851
- Pilewski P, Pommier J, Bergstrom R, Gore W, Howard S, Rabbette M, Schmid U, Hobbs PV, Tsay SC (2003) Solar spectral radiative forcing during SARARI2000. *J Geophys Res* 108(D13):8486
- Prospero JM, Lamb PJ (2003) African droughts and dust transport to the Caribbean: climate change implications. *Science* 302:1024–1027
- Ramanathan V, Crutzen PJ, Kiehl JT, Rosenfeld D (2001) Aerosols, climate, and the hydrological cycle. *Science* 294:2119–2124
- Rosenfeld D (1999) TRMM observed first direct evidence of smoke from forest fires inhibiting rainfall. *Geophys Res Lett* 26:3105–3108
- Rotstajn LD, Penner JE (2001) Indirect aerosol forcing, quasi forcing, and climate response. *J Clim* 14:2960–2975
- Seinfeld JH, Pandis SN (1998) *Atmospheric chemistry and physics: from air pollution to climate change*. Wiley, New York
- Sinha P, Hobbs PV, Yokelson RJ, Bertschi IT, Blake DR, Simpson IJ, Gao S, Kirchstetter TW, Novakov T (2003) Emissions of trace gases and particles from savanna fires in southern Africa. *J Geophys Res* 108(D13):8487
- Stier P, Feichter J, Kinne S, Kloster S, Vignati E, Wilson J, Ganzeveld L, Tegen I, Werner M, Balkanski Y, Schulz M, Boucher O (2004) The aerosol-climate model ECHAM5-HAM. *Atmos Chem Phys* 4:5551–5623

- Tegen I, Lacis AA, Fung I (1996) The influence of climate forcing of mineral aerosols from disturbed soils. *Nature* 380:419–422
- Twomey S (1977) The influence of pollution on the shortwave albedo of clouds. *J Atmos Sci* 34:1149–1152
- Whitehall K (2003) The emissions of biomass burning aerosols in the tropics and their radiative impacts. M.Sc. thesis, Meteorol. Dept. Univ. Reading, 80 pp
- Wong S, Dessler AE, Colarco PR, dsSilva A (2007) The instability associated with the cross-Atlantic transport of Saharan dust and its meteorological implications. *Proc. AMS Conf. Atmos. Chem., Austin*, J7.8
- Ziemke JR, Chandral S, Bhartia PK (2005) A 25-year data record of atmospheric ozone in the pacific from Total Ozone Mapping Spectrometer (TOMS) cloud slicing: implications for ozone trends in the stratosphere and troposphere. *J Geophysical Res* 110:D15105. doi:[10.1029/2004JD005687](https://doi.org/10.1029/2004JD005687)